ELSEVIER

Journal of Hazardous Materials B124 (2005) 44–52

Journal of Hazardous Materials

www.elsevier.com/locate/jhazmat

Mathematical modeling of wire-duct single-stage electrostatic precipitators

M.R. Talaie *

Chemical Engineering Department, Isfehan University, Isfehan, Iran

Received 16 October 2004; received in revised form 17 January 2005; accepted 17 January 2005
Available online 17 May 2005

Abstract

A two-dimensional mathematical model was developed to simulate the performance of wire-duct single-stage electrostatic precipitators (ESP). The model presented by Talaie et al. [M.R. Talaie, M. Taheri, J. Fathikaljahi, A new method to evaluate the voltage–current characteristics applicable for a single-stage electrostatic precipitator, J. Electrostat., 53 (3) (2001) 221–233] was used for prediction of electric field strength distribution and *V–I* characteristic for high-voltage wire-plate configuration. Simple Lagrangian approach was used to predict particle movement. Normal k–ε turbulent flow model with considering electrical body force due to ion and charged particle flow was used to evaluate gas velocity distribution. Ignoring the effect of particle movement and fluid flow, the results of electrical part of mathematical model are in good agreement with experimental data of Penny and Matick [G.W. Penny, R.E. Matrick, Potential in DC corona field, Trans. AIEE Part 1, 79 (1960) 91–99]. The prediction of corona sheath radius and its variation with particle loading and applied voltage is the main distinguishing feature of the present model. This fact was not included in the earlier models.

Keywords: Mathematical modeling; Electrostatic precipitator; Corona discharge

1. Introduction

Electrostatic filters can be the most economical and effective devices to capture fine particulate from a gas stream depending on gas flow rate and requested emission limits. Single-stage electrostatic filters are commonly used in industrial applications. In single-stage ESP charging of particles occurs by using high-voltage power in wire-plate configuration. Although simple wire-duct configurations are seldom used for industrial purposes, they can be a good starting point for developing theoretical model and parametric study of an industrial ESP. Due to applied high-voltage an electric field is created and corona regions are generated around the wires. In these corona zones ions are produced and are driven to the plate as a result of electric field. Ion flow charges particles by bombardments and diffusion to the particle surface. Then charged particles are conducted to the plate due to electrical force. The presence of charged particles and ions over the space between plate and wires reduce thickness of corona zones and ionic current toward the plate. Any mathematical model to evaluate single-stage electrostatic precipitator performance comprises the evaluations of electrical, fluid flow and particle movement parameters. *V–I* characteristics and electrical field strength are the most important electrical parameters, which affect particle collection. The main governing equations for electrical part of ESP models are Poisson equation of electric potential and electrical current continuity equation. Four different techniques (finite difference, finite element, method of characteristic and finite volume) can be identified in literature to solve these equations. In order to use these methods, one needs ion space charge density at the edge of corona. Using Kaptzov assumption has been the most common strategy to estimate this parameter. According to this assumption electrical field strength at the edge of corona is independent of applied voltage above the corona onset voltage. Cristina et al. [2] have solved both governing equations using finite element method. Aboelsaad et al. [3] have modified

* Tel.: +98 917 3133323; fax: +98 311 7932679.
E-mail address: mrtalaie@eng.ui.ac.ir.

0304-3894/$ – see front matter © 2005 Elsevier B.V. All rights reserved.
doi:10.1016/j.jhazmat.2005.01.007

Nomenclature

Ac	Total surface area of collecting plate, m^2
b_i	Ion mobility, m^2/sV
Cc	Kunningham correction factor
C_P	Number concentration of particles with diameter D_P, No./m^3
$C_P(D_P)$	Number concentration frequency distribution of particle size, No./m^4
$C_{P0}(D_P)$	Number concentration frequency distribution of particle size for inlet particles, No./m^4
$C_{Pm}(D_P)$	Mass concentration frequency distribution of particle size, kg/m^4
C_{Pt0}	Total number concentration of inlet particles, No./m^3
C_{Ptm0}	Total mass concentration of inlet particles, kg/m^3
Cu	Average electrical current density at collecting plat, C/m^2
D_P	Particle diameter, m
D_{PM}	Mean diameter of inlet particles, m
e	Elementary charge
E	Electric field strength, V/m
E_{chg}	Charging electric field strength, V/m
E_0	Corona initiating electric field, V/m
E_r	Electrical field in r direction, V/m
E_x	Electrical field in x direction, V/m
E_y	Electrical field in y direction, V/m
f	Roughness factor in Peek's formula, dimensionless
k	Turbulence kinetic energy, J/s/kg
K	Boltzmann constant
m_P	Mass of particle having size D_P, kg
P	Pressure, atm
P_{ref}	Reference pressure, atm
Q_P	Electric charge of particles having diameter between D_P and $D_P + dD_P$, C
s r	Radial direction, m
r_0	Radius of corona sheath, m
r_w	Radius of wire, m
S_i	Source term in ion continuity equation C/s m^3
S_P	Sink term in ion continuity equation C/s m^3
T	Temperature, K
T_{ref}	Reference temperature, K
U	Fluid velocity vector
u	x-Component fluid velocity, m/s
u_P	x-Component particle velocity, m/s
v	y-Component fluid velocity, m/s
v_P	y-Component particle velocity, m/s
x	x-Direction, m
y	y-Direction, m

Greek letters

ρ_f	Fluid density, kg/m^3
ρ_i	Ion charge density, C/m^3
ρ_{i0}	Ion charge density at corona edge, C/m^3
ρ_{pa}	Particle density, kg/m^3
ρ_P	Particle charge density, C/m^3
ε	Turbulence dissipation rate, J/s/kg
ε_0	Permittivity of free air, 8.854×10^{-6} F/m
ε_p	Relative permittivity, dimensionless
ϕ	Electric potential, V
ϕ_A	Applied voltage, V
ϕ_0	Electric potential at corona edge, V
δ	$T_{ref}P/TP_{ref}$, dimensionless
μ	Laminar viscosity, kg/ms
μ_t	Turbulent viscosity, kg/ms
σ	Standard deviation of inlet particle size distribution
η	Particle removal efficiency, wt%

the Kaptzov assumption by multiplying a function of applied voltage at Peek's formula for corona onset voltage. Then, they have solved governing equations using finite element method. Cristina and Feliziani [4] have investigated the influence of dust loading and electric field approximately. Davis and Hoburg [5] have used finite element and characteristics to solve Poisson and ion continuity equations, respectively. McDonald et al. [6] has used finite difference method to solve both governing equations. Zamany [7] has used this model as a part of thorough ESP model to predict ESP performance. Kalio and Stock [8] have used the same strategy as McDonald et al. [6] but they used finite element method to solve Poisson equation. Choi and Fletcher [9] have used finite volume method to solve ion continuity equation. Also they have used k–ε turbulent model and simple Lagrangian approach to evaluate ESP performance. Talaie et al. [1] have presented a new strategy without considering Kaptzov assumption to evaluate electrical field strength distribution and V–I characteristics. In the present work, this method along with the related equations for predicting fluid flow and particle movement were used to show the applicability of this electrical model in simulating single-stage electrostatic precipitator performance.

2. Mathematical model

2.1. Particle movement

Particle movement and particle concentration distribution were determined by using Lagrangian approach. Because in the present model the emphasis was on modification of electrical part of the whole model, simple Lagrangian approach was used to determine particle movement and particle

concentration. This approach is based on tracking of individual particles from inlet to outlet of the ESP channel. In this study, the trajectories of 1500 particles, which were supposed to be located at starting points aligning at the inlet of the channel, were evaluated by using the following equations expressing unsteady-state particle momentum balance along with trajectories:

$$\begin{cases} \dfrac{\mathrm{d}u_\mathrm{P}}{\mathrm{d}t} = \dfrac{3\rho_\mathrm{f}}{4D_\mathrm{P}\rho_\mathrm{Pa}} C_\mathrm{Df}\,|U-U_\mathrm{P}|\,(u-u_\mathrm{P}) + \dfrac{Q_\mathrm{P}(D_\mathrm{P})}{m_\mathrm{P}}E_x, \\ \dfrac{\mathrm{d}x}{\mathrm{d}t} = u_\mathrm{P} \\ \dfrac{\mathrm{d}v_\mathrm{P}}{\mathrm{d}t} = \dfrac{3\rho_\mathrm{f}}{4D_\mathrm{P}\rho_\mathrm{Pa}} C_\mathrm{Df}\,|U-U_\mathrm{P}|\,(v-v_\mathrm{P}) + \dfrac{Q_\mathrm{P}(D_\mathrm{P})}{m_\mathrm{P}}E_y, \\ \dfrac{\mathrm{d}y}{\mathrm{d}t} = v_\mathrm{P} \end{cases} \tag{1}$$

The correlation of Sartor and Abbott [10] for drag coefficient was applied in the present model:

$$\begin{cases} C_\mathrm{Df} = \dfrac{24}{\mathrm{Cc}Re_\mathrm{P}} \quad Re_\mathrm{P} < 0.1 \\ C_\mathrm{Df} = \dfrac{24}{\mathrm{Cc}Re_\mathrm{P}}(1+0.0916Re_\mathrm{P}) \quad 0.1 < Re_\mathrm{P} < 5.0 \\ C_\mathrm{Df} = \dfrac{24}{\mathrm{Cc}Re_\mathrm{P}}(1+0.158Re_\mathrm{P}^{2/3}) \quad 5.0 < Re_\mathrm{P} < 1000 \end{cases} \tag{2}$$

where Cc is Cunningham correction factor which can be calculated using $\mathrm{Cc} = 1+\mathrm{Kn}[\gamma_1 + \gamma_2 \times \exp(-\gamma_3/\mathrm{Kn}]$ [11], with $\mathrm{Kn} = 2\lambda/D_\mathrm{P}$, $\gamma_1 = 1.231$, $\gamma_2 = 0.4695$, $\gamma_3 = 1.1783$ and λ which is mean free path of molecules and can be taken equal to 65 nm for ESP operational conditions. This correction factor is 1.16 and 1.08 for particles having size 1 and 2 μm, respectively.

The particles, which hit the collecting wall, are assumed to be collected as particle layer. The efficiency of ESP was evaluated by computing the fraction of collected particles. In order to calculate the particle concentration distribution the PSI-CELL model was modified to include the effect of particle size distribution. The conventional form of PSI-CELL model is as follows [12]:

$$C_\mathrm{P} = \sum_{j=\mathrm{ni}}^{\mathrm{nf}} \frac{n_j \tau_j}{V_\mathrm{C.V.}} \tag{3}$$

where ni to nf are the trajectories passing a control volume which has the volume of $V_\mathrm{C.V.}$, n_j is number flow rate of particles at point j located along the vertical line at enterance and τ_j is the residence time of particles in the control volume through the trajectory j. Using assumption that the number flow rate of particles located at point j is constant along their trajectory, the Eq. (3) can be written in the following form:

$$C_\mathrm{P} = \sum_{j=\mathrm{ni}}^{\mathrm{nf}} \frac{u_{\mathrm{P}0j}\Delta_{\mathrm{P}0j} C_{\mathrm{P}0j}\tau_j}{V_\mathrm{C.V.}} \tag{4}$$

where $u_{\mathrm{P}0j}$ and $C_{\mathrm{P}0j}$ are the initial velocity and number concentration of particles located at point j and $\Delta_{\mathrm{P}0j}$ is the length increment selected for this location. The modifiation used by Talaie et al. [13] for including particle size distribution was applied in the present model. As a result of this modification the following equation to evaluate number frequency distribution of particle size was obtained:

$$C_\mathrm{P}(D_\mathrm{P}) = \sum_{j=\mathrm{ni}}^{\mathrm{nf}} \frac{u_{\mathrm{P}0j}\Delta_{\mathrm{P}0j} C_{\mathrm{P}0j}(D_\mathrm{P})\tau_j}{V_\mathrm{C.V.}} \tag{5}$$

where $C_{\mathrm{P}0j}(D_\mathrm{P})$ is the number concentration frequency distribution of particle size at beginning of trajectory j ($C_{\mathrm{P}0j}(D_\mathrm{P})\,\mathrm{d}D_\mathrm{P}$ is number concentration of particles having size between D_P and $D_\mathrm{P} + \mathrm{d}D_\mathrm{P}$).

In this model the effects of gas turbulence on particle movement is ignored and mean gas velocity was used for calculations.

2.2. Fluid flow

In order to predict fluid velocity distribution, the normal k–ε turbulent flow model was used. For two-dimensional incompressible steady flow with considering electrical body force, the equations describing momentum and mass balance are as follows:

$$\frac{\partial}{\partial x}\left[\rho_\mathrm{f}u^2 - (\mu+\mu_\mathrm{t})\frac{\partial u}{\partial x}\right] + \frac{\partial}{\partial y}\left[\rho_\mathrm{f}uv - (\mu+\mu_\mathrm{t})\frac{\partial u}{\partial y}\right] = -\frac{\partial p}{\partial x} + \frac{\partial}{\partial x}\left(\mu_\mathrm{t}\frac{\partial u}{\partial x}\right) + \frac{\partial}{\partial y}\left(\mu_\mathrm{t}\frac{\partial v}{\partial x}\right) + f_{\mathrm{i}x} + f_{\mathrm{P}x} \tag{6}$$

$$\frac{\partial}{\partial x}\left[\rho_\mathrm{f}uv - (\mu+\mu_\mathrm{t})\frac{\partial v}{\partial x}\right] + \frac{\partial}{\partial y}\left[\rho_\mathrm{f}v^2 - (\mu+\mu_\mathrm{t})\frac{\partial v}{\partial y}\right] = -\frac{\partial p}{\partial y} + \frac{\partial}{\partial x}\left(\mu_\mathrm{t}\frac{\partial u}{\partial y}\right) + \frac{\partial}{\partial y}\left(\mu_\mathrm{t}\frac{\partial v}{\partial y}\right) + f_{\mathrm{i}y} + f_{\mathrm{P}y} \tag{7}$$

$$\frac{\partial(\rho_\mathrm{f}u)}{\partial x} + \frac{\partial(\rho_\mathrm{f}v)}{\partial y} = 0 \tag{8}$$

$$\frac{\partial}{\partial x}(\rho_\mathrm{f}uk) + \frac{\partial}{\partial y}(\rho_\mathrm{f}uk) = \frac{\partial}{\partial x}\left(\frac{\mu_\mathrm{t}}{\sigma_k}\frac{\partial k}{\partial x}\right) + \frac{\partial}{\partial y}\left(\frac{\mu_\mathrm{t}}{\sigma_k}\frac{\partial k}{\partial y}\right) + \mu_\mathrm{t}G - C_\mathrm{D}\rho_\mathrm{f}\varepsilon \tag{9}$$

$$\frac{\partial}{\partial x}(\rho_\mathrm{f}u\varepsilon) + \frac{\partial}{\partial y}(\rho_\mathrm{f}u\varepsilon) = \frac{\partial}{\partial x}\left(\frac{\mu_\mathrm{t}}{\sigma_\varepsilon}\frac{\partial \varepsilon}{\partial x}\right) + \frac{\partial}{\partial y}\left(\frac{\mu_\mathrm{t}}{\sigma_\varepsilon}\frac{\partial \varepsilon}{\partial y}\right) + \frac{\varepsilon}{k}(C_1\mu_\mathrm{t}G - C_2\rho_\mathrm{f}\varepsilon) \tag{10}$$

$$G = 2\left(\frac{\partial u}{\partial x}\right)^2 + 2\left(\frac{\partial v}{\partial y}\right)^2 + \left(\frac{\partial u}{\partial y} + \frac{\partial v}{\partial x}\right)^2 \tag{11}$$

$$\mu_t = C_\mu \frac{\rho_f k^2}{\varepsilon} \tag{12}$$

In the momentum equations, f_{ix} and f_{iy} are x and y components of electrical force exerted to the ions and f_{Px} and f_{Py} are x and y components of force exerted due to drag force between particles and fluid.

The parameters used in normal k–ε model is as follows:

σ_k	σ_ε	C_μ	C_D	C_1	C_2
1.0	1.3	0.09	1.0	1.44	1.92

2.3. Electrical body forces

The electrical body force due to presence of ions can be found by the following equation:

$$\begin{cases} f_{ix} = \rho_i E_x \\ f_{iy} = \rho_i E_y \end{cases} \tag{13}$$

The body force frequency distribution of particle size due to particle movement was calculated by the following equation:

$$\begin{cases} f_{Px}(D_P) = -\displaystyle\sum_{j=n_{Pi}}^{n_{Pf}} \frac{u_{P0j}\Delta_{Pj}C_{P0j}(D_P)\tau_j}{V_{C.V.}} \\ \quad \times \dfrac{1}{2}\dfrac{\pi}{4} D_P^2 \rho_f C_{Df} |U - U_P| (u - u_P) \\ f_{Py}(D_P) = -\displaystyle\sum_{j=n_{Pi}}^{n_{Pf}} \frac{u_{P0j}\Delta_{Pj}C_{P0j}(D_P)\tau_j}{V_{C.V.}} \\ \quad \times \dfrac{1}{2}\dfrac{\pi}{4} D_P^2 \rho_f C_{Df} |U - U_P| (v - v_P) \end{cases} \tag{14}$$

Total body force can be evaluated by integrating the above equation for all particle size as follows:

$$\begin{cases} f_{Px} = \displaystyle\int_{D_{P\min}}^{D_{P\max}} f_{Px}(D_P) \mathrm{d}D_P \\ f_{Py} = \displaystyle\int_{D_{P\min}}^{D_{P\max}} f_{Py}(D_P) \mathrm{d}D_P \end{cases} \tag{15}$$

2.4. Electrical field

The equation used to determine the electric potential was the Poisson equation, which in two-dimensional form can be written as follows:

$$\frac{\partial^2 \phi}{\partial x^2} + \frac{\partial^2 \phi}{\partial y^2} = -\frac{(\rho_i + \rho_P)}{\varepsilon_0} \tag{16}$$

The electric field can be obtained from electric potential by the following equation:

$$\begin{cases} -\dfrac{\partial \phi}{\partial x} = E_x \\ -\dfrac{\partial \phi}{\partial y} = E_y \end{cases} \tag{17}$$

2.5. Ion charge density and V–I characteristic

The following continuity equation of electric charge was used to obtain ion charge density distribution:

$$\frac{\partial(\rho_i b_i E_x + u\rho_i)}{\partial x} + \frac{\partial(\rho_i b_i E_y + v\rho_i)}{\partial y} = D_i \left(\frac{\partial^2 \rho_i}{\partial x^2} + \frac{\partial^2 \rho_i}{\partial y^2} \right) + S_i + S_P \tag{18}$$

where D_i is ion diffusion coefficient, ρ_i is ion charge density, S_i is the source term (positive), which represents the rate of ion generation in corona zone per unit of volume, S_P is the sink term (negative), which represents the rate of ion consumption due to particle charging per unit of volume.

The source term was calculated by the following equation for the control volumes surrounding the wires and was set to be zero for the others:

$$S_i = \frac{\pi r_0 E_0 b_i \rho_{i0}}{\Delta x \Delta y} \tag{19}$$

The sink term S_P was calculated by the following equation expressing the charge balance for particles over a control volume:

$$S_P = \sum_{C.S.} u_{P0j}\Delta_{P0j} \int_{D_{P\min}}^{D_{P\max}} C_{P0j}(D_P) Q_{Pj} \mathrm{d}D_P \tag{20}$$

where Q_{Pj} is the electric charge of particles having diameter D_P, in trajectory located at point j and varies along this trajetoriy and indice C.S. means that the values are calculated at control surfaces (output with negative sign and input with positive sign must to be considered).

The strategy developed by Talaie et al. [1] to find ion space charge at the edge of corona, ρ_{i0}, is explained in the following section.

The grid of control volumes is selected so that each wire and its corona zone is encircled by a control volume completely. Around the wires Gauss's equation in cylindrical coordinate was used to predict the electric potential:

$$\frac{\partial(rE_r)}{\partial r} = 0 \tag{21}$$

Although in the above equation electric field induced by ion charge is neglected, it can be used for prediction of electric field around the wires for small radius. It is due to the fact that the effect of charge on electric field depends on radial distance from center and for small radius it can be neglected.

By integrating the above equation, the following relation was obtained:

$$rE_r = \text{Cons.} \tag{22}$$

Corona sheath radii were found for south, east and west directions by solving the following equations resulted from combining Eq. (22) and Peek's formula for corona initiating

electric field:

$$\begin{cases} r_0 f \quad 3\times10^6\left(\delta+0.03\sqrt{\dfrac{\delta}{r_0}}\right)=r_y\left|E_{y_j}\right| & \text{For south direction} \\ r_0 f \quad 3\times10^6\left(\delta+0.03\sqrt{\dfrac{\delta}{r_0}}\right)=\dfrac{r_x\left|E_{x_i}\right|}{\mathrm{Cos}\theta} & \text{For west direction} \\ r_0 f \quad 3\times10^6\left(\delta+0.03\sqrt{\dfrac{\delta}{r_0}}\right)=\dfrac{r_x\left|E_{x_{i+1}}\right|}{\mathrm{Cos}\theta} & \text{For east direction} \end{cases} \tag{23}$$

where $\mathrm{Cos}\theta=(\Delta x/2)/r_x$ as shown in Fig. 1 and f is roughness factor which can be considered unity for smooth wire. The radius of the corona sheath, r_0, will be the average of these three calculated values.

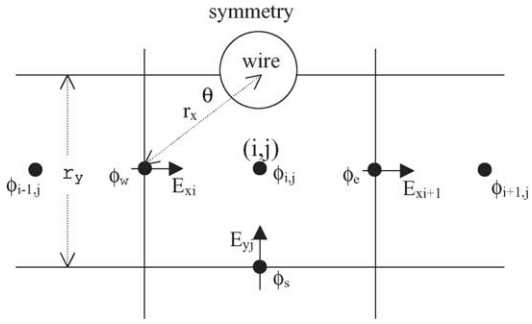

Fig. 1. Demonstrative scheme of the control volume surrounding a wire.

The value of ion charge density at corona edge, ρ_{i0}, was evaluated by the following empirical equation developed by Talaie et al. [1]:

$$\begin{cases} \dfrac{\rho_{i0}r_0^2}{\varepsilon_0(\phi_A-\phi_0)}=\left(\dfrac{r_0-r_w}{r_w}\right) & \text{For positive corona} \\ \dfrac{\rho_{i0}r_0^2}{\varepsilon_0(\phi_A-\phi_0)}=\left(\dfrac{r_0-r_w}{r_w}\right)^2 & \text{For negative corona} \end{cases} \tag{24}$$

After solving the above equations, average electrical current density at the plate was obtained by:

$$\mathrm{Cu}=\left.\frac{\oint b_i\rho_i E_y \mathrm{d}A_C+\sum_{\mathrm{C.P.}}u_{P0j}\Delta_{P0j}\int_{D_{P\min}}^{D_{P\max}}C_{P0j}(D_P)Q_{Pj}\,\mathrm{d}D_P}{A_C}\right|_{\mathrm{wall}} \tag{25}$$

where C.P. means collecting plate.

2.6. Particle charge density

Particle charge frequency distribution of particle size was calculated by the following equation:

$$\rho_P(D_P)=\sum_{j=\mathrm{ni}}^{\mathrm{nf}}\frac{u_{P0j}\Delta_{P0j}C_{P0j}(D_P)Q_{Pj}\tau_j}{V_{\mathrm{C.V.}}} \tag{26}$$

Particle charging occurs based on two field and diffusion charging mechanisms. For particles larger than 0.5 μm adequately and higher applied voltage, field charging is dominant. In intermediate cases both mechanisms are significamt and for estimating particle charging the models that combine both mechanisms must be used. In this work, the model developed by lawless [14] was used to predict particle charging. Nonethelese, for particles having the size larger than 0.5 μm enough using field charging model alone gives the same results. Lawless's model can be described as follows:

$$\frac{\mathrm{d}Q_P}{\mathrm{d}t}=\begin{cases} \rho_i b_i\dfrac{Q_{\mathrm{sat}}}{4\varepsilon_0}\left(1-\dfrac{Q_P}{Q_{\mathrm{sat}}}\right)^2 & Q_P\le Q_{\mathrm{sat}}+a(\tilde{E})\dfrac{8\pi\varepsilon_0 KT}{e}\dfrac{\rho_i b_i D_P}{4\varepsilon_0} \\ \dfrac{a(E)\rho_i b_i}{\varepsilon_0}\dfrac{Q_P-Q_{\mathrm{sat}}}{\exp\left\{\dfrac{(Q_P-Q_{\mathrm{sat}})e}{2\pi\varepsilon_0 KTD_P}\right\}} & Q_P\succ Q_{\mathrm{sat}} \end{cases} \tag{27}$$

where Q_{sat} is saturation charge of a particle and is given by the following equation:

$$Q_{\mathrm{sat}}=\frac{3\varepsilon_P}{1+\varepsilon_P}\pi\varepsilon_0 D_P^2 E_{\mathrm{chg}} \tag{28}$$

The parameter $a(\tilde{E})$ can be determine using the following equation:

$$a(\tilde{E})=\begin{cases}\dfrac{1}{(\tilde{E}+0.457)^{0.575}} & \tilde{E}\ge0.525 \\ 1 & \tilde{E}\prec0.525\end{cases} \tag{29}$$

where:

$$\tilde{E}=\frac{D_P E_{\mathrm{chg}}e}{2KT} \tag{30}$$

Total particle charge density at each point can be calculated by using the following equation:

$$\rho_P=\int_{D_{P\min}}^{D_{P\max}}\rho_P(D_P)\mathrm{d}D_P \tag{31}$$

3. Method of solution

The equations of k–ε turbulent flow model were solved using SIMPLER algorithm. Equation of electric potential was solved using finite difference method. Ion continuity equation was solved using power-law scheme of control volume method. A grid of 150×40 was used to solve all above

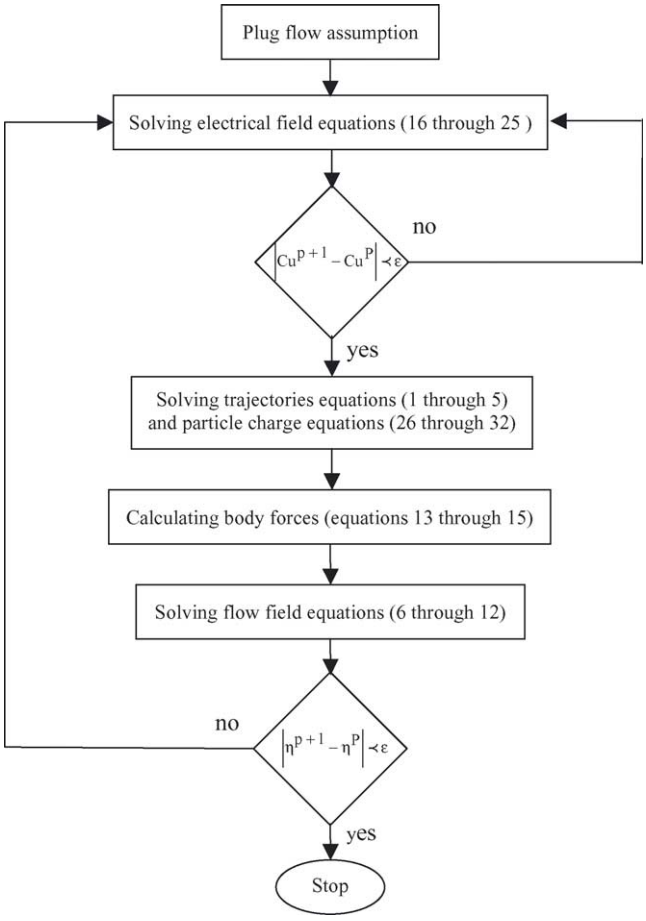

Fig. 2. Algorithm developed for performing calculations.

equations. The generated grid was compacted near the collecting wall and was modified in such a way that each wire and its corona zone were set inside a single control volume completely. An excellent discussion about control volume method and algorithms for solution of fluid flow equations can be found in Ref. [15]. The differential equations of particle trajectories and particle charging were solved using forth-order Runge-Kutta method. All integrals appeared in the present model was solved using fifth-order Gauss-Quadrature method.

The algorithm developed for performing these calculations is shown in Fig. 2.

4. Results

In order to validate the electrical model experimental data of Penny and Matick [16] was used. This experiment has been performed for a high-voltage negative-corona wire-plate configuration in the absence of charged particles. Fig. 3 shows the current–voltage characteristic curve for negative corona and comparison of calculated results with the experimental data. The good agreement between the results of the model and experimental data justifies using this electrical model as

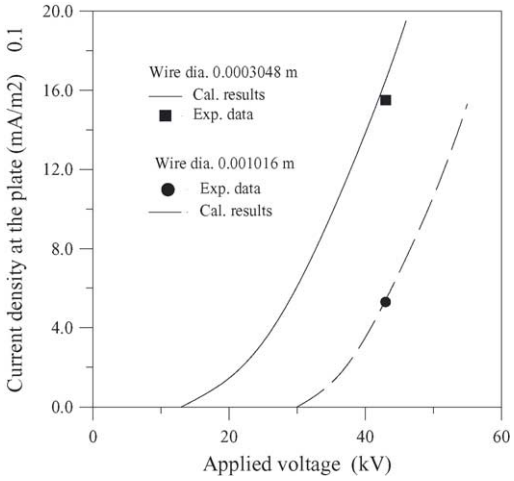

Fig. 3. Current–voltage characteristics curve, comparison between the results and experimental data of Penny and Matick [16]. Wire-plate distance: 0.1143 m, wire–wire distance: 0.14696 m and negative corona.

a part of overall mathematical model for simulation of electrostatic precipitator performance. In order to investigate the effect of operating parameters on ESP performance and examine the capability of the present model, ESP configuration shown in Fig. 4 was considered.

Fig. 5 shows the effect of secondary flow due to ion movement towards collecting plate on removal efficiency. This figure shows the comparison between removal efficiency calculated based on plug flow and velocity distribution predicted by the model. Apparently, decreasing gas velocity increases the difference between two curves due to increasing secondary flow. The results of the model show that secondary flow almost has negative effect on particle removal efficiency.

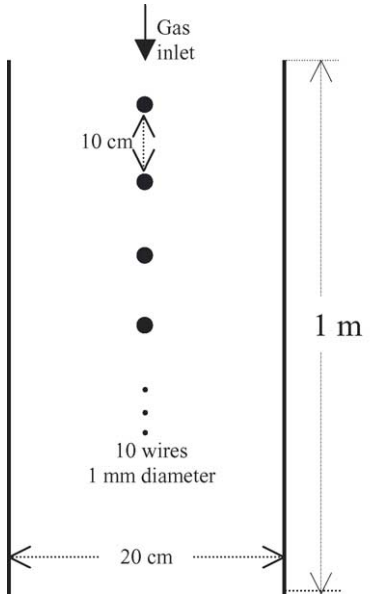

Fig. 4. The configuration of ESP used for simulation. Other specifications are: $\rho_P = 2350\,kg/m^3$, $\varepsilon_P = 3.5$, $T = 25\,^{\circ}C$ and $P = 1$ atm.

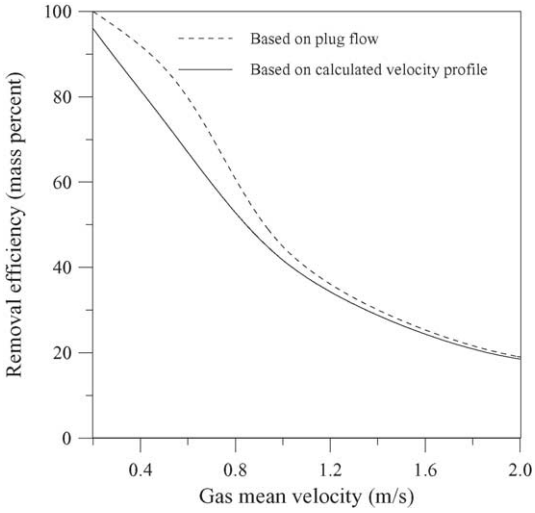

Fig. 5. The effect of secondary flow on particle removal efficiency, $\phi_A = 30$ kV, monodisperse particle loading, $C_{Pm0} = 10$ g/m^3, $D_P = 3$ μm.

Figs. 6 and 7 show the comparison between mass flow rate frequency distribution of inlet and outlet particles for mean gas velocity of 0.5 and 1.0 m/s respectively. Inlet distribution is based on log-normal population distribution with mean diameter (D_{PM}) of 5 μm and standard deviation (σ) of 1.3. The areas under these curves are equal to the mass flow rates of inlet and outlet particles.

Fig. 8 shows the effect of inlet particle loading on particle removal efficiency. As can be seen, increasing particle concentration decreases collection efficiency. It can be attributed to the effect of particle charge on *V–I* characteristic. In the absence of particle charge, the mean corona sheath thickness and ionic current increase as applied voltage increases. For high particle concentration, charged particles cause to

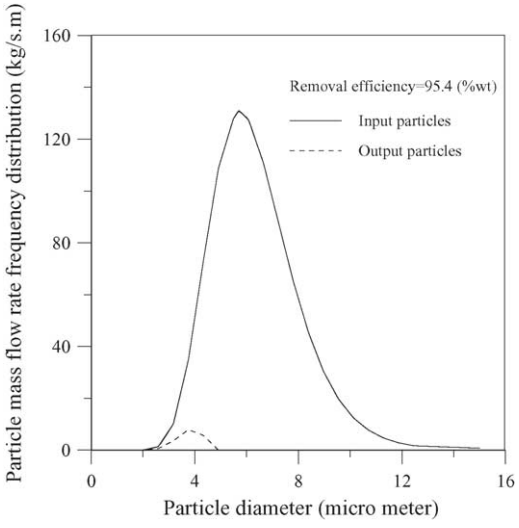

Fig. 6. Comparison between particle mass flow rate frequency distribution ($f_{con}dD_P$ = mass flow rate of particles having size between D_P and $D_P + dD_P$) of inlet and outlet, $u_0 = 0.5$ m/s, $\phi_A = 25$ kV, polydisperse particle loading, $C_{Pm0} = 10$ g/m^3, $D_{PM} = 5$ μm, $\sigma = 1.3$.

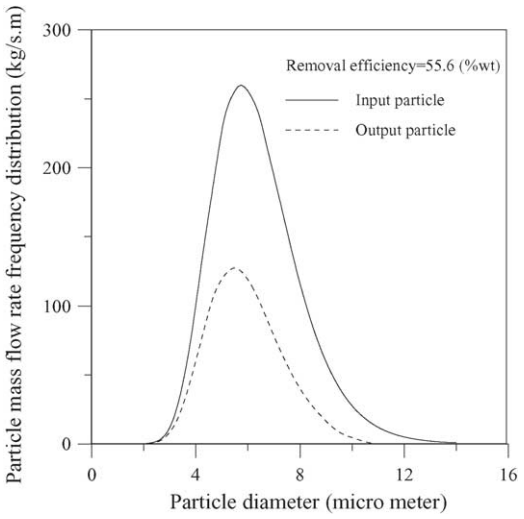

Fig. 7. Comparison between particle mass flow rate frequency distribution ($f_{con}dD_P$ = mass flow rate of particles having size between D_P and $D_P + dD_P$) of inlet and outlet, $u_0 = 1.0$ m/s, $\phi_A = 25$ kV, polydisperse particle loading, $C_{Pm0} = 10$ g/m^3, $D_{PM} = 5$ μm, $\sigma = 1.3$.

reduce both corona sheath radius and ionic current. Reducing ionic current decreases particle charging and hence particle removal efficiency.

Fig. 9 shows the effect of particle loading and applied voltage on mean corona sheath radius. The results noted as set 1, are for applied voltage 20 kV in the absence of particle charge. The main reason for different values of corona sheath radius around different wires is the end effect of ESP channel. Sets 2 and 3 data were obtained for applied voltage of 30 and 40 kV. As it was expected increasing applied voltage increases corona sheath radius in the absence of charged particles. Sets 4–6 were attained for applied voltage of 40 kV and particle loading of 1, 10 and 50 g/m^3. For set 6, the corona circle radius is high for first wire and reduces to wire radius

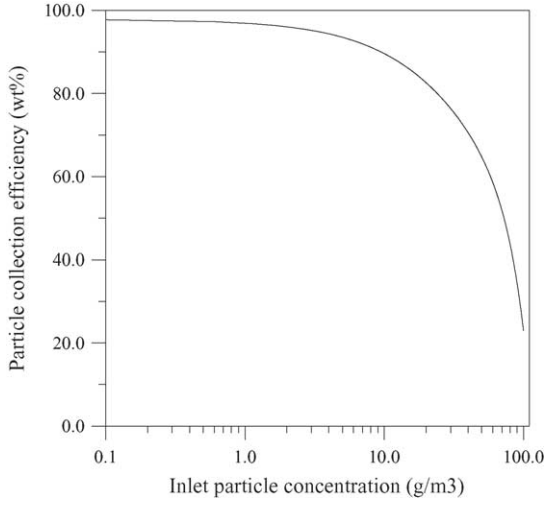

Fig. 8. The effect of particle loading on particle removal efficiency, monodispersed particle loading with $D_P = 5$ μm, $\phi_A = 30$ kV, $u_0 = 2$ m/s and wire diameter of 1 mm.

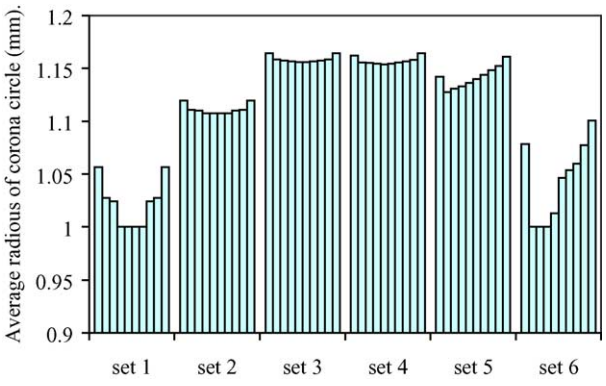

Fig. 9. The effect of applied voltage and inlet particle concentration on corona zone thickness around the 10 wires located through the ESP channel. set 1: $\phi_A = 20$ kV, $C_{Ptm0} = 0$ g/m^3; set 2: $\phi_A = 30$ kV, $C_{Ptm0} = 0$; set 3: $\phi_A = 40$ kV, $C_{Ptm0} = 0$; set 4: $\phi_A = 40$ kV, $C_{Ptm0} = 1$ g/m^3; set 5: $\phi_A = 40$ kV, $C_{Ptm0} = 10$ g/m^3; set 6: $\phi_A = 40$ kV, $C_{Ptm0} = 50$ g/m^3; All data are based on monodispersed particle loading with $D_P = 5$ μm and wire diameter of 1 mm.

suddenly. It is due to particle charging time. Particles entering ESP channel are charged as they move through channel. Apparently, increasing particle loading reduces the corona zone thickness. However, as particles pass through the ESP channel corona zone thickness around the wires increase due to collection of particles and decreasing of particle concentration. This fact is more obvious for higher particle loadings (50 g/m^3). It should be mentioned when the radius of corona zone will be equal to wire radius there is not any corona discharge from this wire. However it dose not mean complete corona quenching and corona discharge can be continues by active zone created around other wires.

Fig. 10 shows the variation of ionic current with inlet particle concentration. Expectedly, increasing particle concentration decreases ionic current as a result of electric field induced by particle charge. The presence of charged particles causes to reduce corona sheath thickness around the wires and

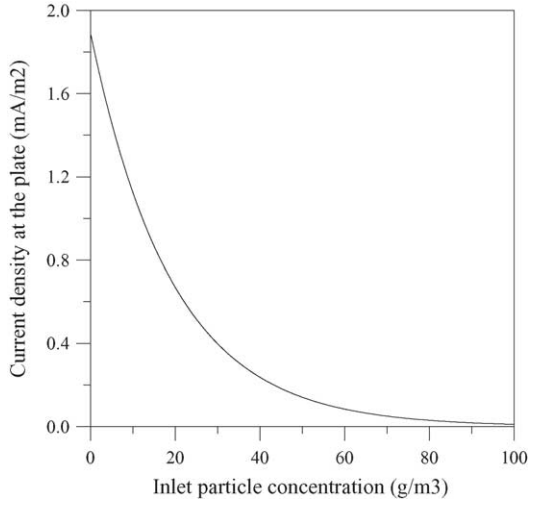

Fig. 10. The effect of particle loading on average ionic current density, monodispersed particle loading with $D_P = 5$ μm, $\phi_A = 30$ kV, $u_0 = 2$ m/s and wire diameter of 1 mm.

ion charge density at corona edge. This effect decreases ion current emitted from the corona zones.

5. Conclusion

A mathematical model was developed to simulate single-stage ESP performance. The prediction of corona sheath thickness and its variation with particle loading and applied voltage is the main distinguishing feature of the present model. This fact was not included in the earlier models. The results show that the electrical part of the model can be a useful tool to calculate electrical parameters in a wire-duct ESP. Also the results indicate that considering secondary flow, which can be more significant for the case of higher applied voltage and lower mean gas velocity reduces the calculated removal efficiency. The results also show that for the case of high inlet particle concentration the corona quenching is observed for upstream wires, but for the downstream ones due to collection of particles and reducing particle charge density corona phenomenon can be occurs.

References

[1] M.R. Talaie, M. Taheri, J. Fathikaljahi, A new method to evaluate the voltage–current characteristics applicable for a single-stage electrostatic precipitator, J. Electrostat. 53 (3) (2001) 221–233.
[2] S. Cristina, G. Dinelli, M. Feliziani, Numerical computation of corona space charge and *V–I* characteristics in DC electrostatic precipitators, IEEE Trans. Ind. Appl. 27 (1) (1991) 147–153.
[3] M.M. Aboelsaad, L. Shafai, M.M. Rashwan, Numerical assessment of unipolar corona ionized field quantities using the finite element method, IEEE Proc. 13Ga (2) (1989) 79–86.
[4] S. Cristina, M. Feliziani, Calculation of ionized field in D electrostatic precipitator in the presence of dust and electric wind, IEEE Industry Applications Socciety Annual Meeting, 1991, pp. 616–621.
[5] J.L. Davis, J.F. Hoburg, Wire-duct precipitator field and charge computation using finite element and characteristics methods, J. Electrostat. 14 (1983) 187–199.
[6] J.R. McDonald, B.S. Wallace, H.W. Spencer, L.E. Sparks, A mathematical model for calculating electrical conditions of wire-duct electrostatic precipitation devices, J. Appl. Phys. 48 (6) (1979) 2231–2242.
[7] J. Zamany, Modeling of particle transport in commercial electrostatic precipitators, Ph.D. dissertation, Department of Fluid Mechanics, Technical University of Denmark, 1992.
[8] G.A. Kallio, D.E. Stock, Computation of electrical conditions inside wire-duct electrostatic precipitators using combined finite-element, finite difference technique, J. Appl. Phys. 59 (6) (1986) 1799–1806.
[9] B.S. Choi, C.A.J. Fletcher, Computation of particle transport in an electrostatic precipitator, J. Electrostat. 40 (1) (1997) 413–418.
[10] J.D. Sartor, C.E. Abbott, Prediction and measurement of the accelerated motion of water drops in air, J. Appl. Meteorol. 14 (1975) 232–239.
[11] D.K. Hutchins, M.H. Harper, R.L. Felder, Slip correction measurements for solid spherical particles by modulated dynamic light scattering, Aerosol Sci. Technol. 22 (1995) 202–218.

[12] C.T. Crowe, M.P. Sharma, D.E. Stock, The particle-source-in-cell (PSI-CELL) model for gas-droplet flows, Trans. ASME J. Fluids Eng. (1977) 235.
[13] M.R. Talaie, J. Fathikaljahi, M. Taheri, Mathematical modeling of double-stage electrostatic precipitators based on a modified Eulerian approach, Aerosol Sci. Technol. 34 (2001) 512–519.
[14] P.A. Lawless, Particle charging bounds, symmetry relations and an analytic charging rate model for the continuum regime, J. Aerosol Sci. 27 (1996) 191–215.
[15] S.V. Patanakar, Numerical Heat Transfer and Fluid Flow, Hemisphere publishing, 1980.
[16] G.W. Penny, R.E. Matick, Potentials in DC corona fields, Trans. AIEE. 79 (1) (1960) 91–99.